phys. stat. sol. (a) **171**, 175 (1999)

Subject classification: 61.72.Ss; 71.55.Cn; 78.30.Am; S5.11

Oxygen and Carbon Precipitation in Multicrystalline Solar Silicon

H. J. MÖLLER (a), L. LONG (a), M. WERNER (b), and D. YANG (a)

(a) Institute for Experimental Physics, Technical University Bergakademie Freiberg, Silbermannstr. 1, D-09599 Freiberg, Germany
Tel./Fax: +49-03731-392896/394314; e-mail: moeller@physik.tu-freiberg.de

(b) Max-Planck Institute of Microstructure Physics, Weinberg 2, D-06120 Halle, Germany
Tel./Fax: +49-0345-5582691/5511223; e-mail: m_werner@mpi-halle.mpg.de

(Received October 2, 1998)

Oxygen and carbon are the main impurities in multicrystalline silicon for photovoltaic applications. Precipitation of oxygen and carbon occurs during crystal growth and solar cell processing. Depending on the thermal conditions and the initial oxygen and carbon content various types of SiO_2, SiC precipitates and oxygen related defects are observed and investigated by IR spectroscopy and transmission electron microscopy. Topographic μ-PCD measurements are used to study the minority carrier lifetime in the material locally. It is found that certain types of oxygen defects reduce the lifetime of the bulk and enhance the recombination activity of dislocations. Quantitative measurements of the oxygen precipitation of pre-annealed specimens are carried out to study the oxygen precipitation systematically. A statistical nucleation and growth model using rate equations and a Fokker-Planck equation is applied to simulate the precipitation process numerically.

1. Introduction

Multicrystalline silicon is a low cost material for photovoltaic applications. The solar conversion efficiencies of commercial cells are typically in the range of 12 to 15% and up to about 17% have been obtained by sophisticated solar cell designs. In theory, the potential of multicrystalline or mc-silicon is even higher, possibly up to 20% [1]. Such an improvement of the efficiency would greatly increase the commercial viability. The performance of multicrystalline solar cells is mainly limited by minority carrier recombination at dislocations and intragrain defects such as certain impurities, small clusters of atoms or precipitates. Particularly localized regions of high dislocation densities are known to be rather detrimental [2, 3]. Since recombination at pure dislocations is known to be relatively weak, it has been suggested that in these regions the decoration with metallic impurities or precipitates is responsible for the enhanced recombination [4 to 8]. Recent results indeed indicate that metal impurity agglomeration at dislocations occurs in regions of higher carrier recombination in mc-silicon [9]. Fast diffusing metals such as copper, iron, chromium or nickel that occur in mc-silicon segregate or precipitate at dislocations and grain boundaries after the crystallization of the ingots. During the high temperature steps of the solar cell process, typically in the range of 800 to 1000 °C, the metals are released into the bulk again and partly removed by phosphorous and aluminum gettering which is part of the standard solar cell process. Experimental and theoretical investigations have shown that gettering can be slowed down signifi-

cantly if the dissolution rate of precipitated impurities is slow and rate limiting [3, 4, 10, 11]. It is therefore important to understand the factors that determine the agglomeration and distribution of metal impurities during crystallization and solar cell processing particularly in regions of high dislocation densities. Our investigations in recent years have shown that oxygen plays an important role, particularly oxygen precipitates that are known to getter metal impurities. In combination with dislocations and grain boundaries they could enhance the precipitation of metals at these extended defects. Oxygen and carbon are in fact the main impurities in mc-silicon. The concentrations of oxygen are comparable to Cz-silicon while the carbon concentrations are usually higher in mc-silicon.

Oxygen is known to affect the conversion efficiency of solar cells. Both for Cz- and multicrystalline silicon a degradation of the solar cell performance has been reported [12 to 19] while an improvement has been observed for polycrystalline ribbon material [20]. Oxygen can form a variety of defects that affect the electrical behavior differently. Clusters of a few oxygen atoms and various sizes and crystal structures are observed for larger SiO_2 precipitates [21, 22]. Well-known defects are the Thermal Donors that are clusters of a few oxygen atoms and the New Donors that have been connected with SiO_2 precipitates [23]. In addition, oxygen and carbon can precipitate at grain boundaries and dislocations and also change their electrical behavior. The defects can also have an impact on the bulk carrier recombination and on the properties of the p–n junction if they are large enough to penetrate the space charge region [24]. The evolution of the oxygen defects depends very much on the thermal history of the material and every thermal step between crystal growth and solar cell process has to be considered. Carbon forms defects that are less electrically active but is important because of its ramifications on the oxygen precipitation.

In this paper results are summarized that demonstrate the role of oxygen-induced defects in multicrystalline solar silicon. Furthermore, some results are presented from a systematic study of the oxygen precipitation in polycrystalline silicon under defined conditions. On the basis of these results the precipitation process has been simulated numerically using a chemical rate model that has recently been successfully applied to simulate the oxygen precipitation in mono-silicon [25 to 27]. The fundamental quantity in the model is a size-distribution function of the precipitate, which allows one to simulate the growth and dissolution processes of all precipitates as a function of time and temperature. This model is particularly suitable for multi-step annealing processes when dissolution processes of previously formed precipitates occur. Numerical results for typical two-step annealing processes will be discussed and compared with experimental investigations on mc-silicon.

2. Experimental Procedure

2.1 Specimen preparation and defect characterization

Boron doped multicrystalline silicon for solar cells grown by directional solidification was used for the investigations. The boron concentration was about 2×10^{16} cm^{-3}. The oxygen and carbon concentrations of the wafers varied between 2 to 12×10^{17} cm^{-3} and 0.05 to 5×10^{17} cm^{-3}, respectively. The as-grown wafers were annealed under argon gas at various temperatures between 400 and 1200 °C for 2 to 24 h. Prior to annealing the wafers were cut, polished and chemically cleaned by an RCA process.

The dislocation densities were determined by selective etching on chemomechanically polished surfaces and vary between 10^4 and 10^6 cm^{-2}, locally up to 10^8 cm^{-2}. In addition to large dislocation etch pits also shallow etch pits can be observed in mc-silicon that are due to small precipitates. The density of the shallow etch pits varies between 0 and 10^8 cm^{-2}. The TEM investigations show that at least a substantial part of the shallow etch pits are due to oxygen precipitates. The concentrations of precipitates determined from etch pit investigations agree with the densities determined from TEM investigations within an order of magnitude. The minority carrier lifetime of the specimens was investigated by a topographic microwave photoconductance decay (μ-PCD) technique. The results have been obtained on unpassivated surfaces and include the surface recombination. Therefore the absolute values have to be taken with care but are sufficient for a relative comparison of data.

2.2 FTIR investigations

The concentrations of dissolved oxygen and carbon, and the density, size and morphology of precipitates were determined by FTIR and TEM, respectively. Interstitial oxygen and substitutional carbon are associated with optical absorption lines at 1107 cm^{-1} and 605 cm^{-1}, respectively, in silicon. The concentrations of the elements have been determined from the peak height using the calibration factors: 3.14×10^{17} cm^{-3} and 1.0×10^{17} cm^{-3}, respectively. In addition, a broader line at 1224 cm^{-1} can occur in the spectrum. This line has been associated with oxygen precipitates [28, 29] and explained by the excitation of the LO mode (longitudinal optical phonon) of SiO_2. The LO mode is normally infrared inactive for bulk SiO_2 but can become active for particles that are small enough to become electrically polarized. Calculations of the polarization show that the 1224 cm^{-1} band arises if the particles are smaller than $\lambda/2\pi n_m$, where λ is the wavelength of the incident radiation and n_m the refractive index of the embedding matrix, and have a plate-like shape [29]. The size, density and morphology of the oxygen and of carbon precipitates have been studied and confirmed by TEM.

3. Experimental Results

3.1 As-grown multicrystalline silicon

The typical crystallization process of a multicrystalline ingot takes about 40 to 60 h. During solidification the planar melt interface moves from the bottom to the top of the

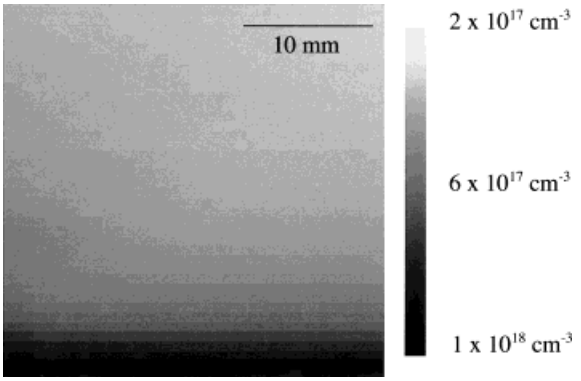

Fig. 1. Topogram of the vertical distribution of interstitial oxygen in a multicrystalline silicon ingot. The local oxygen concentration was determined by FTIR using the absorbance line at 1107 cm^{-1}

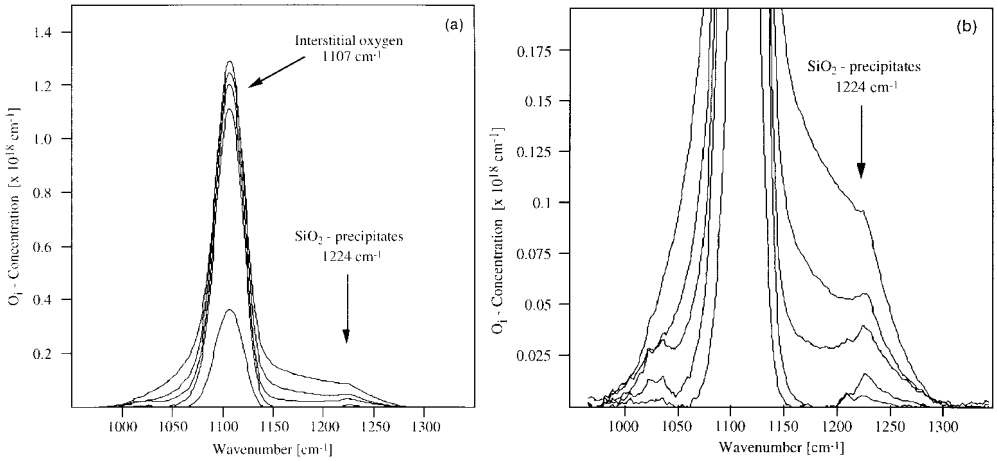

Fig. 2. FTIR spectrum of oxygen at various positions in a mc-silicon ingot. The spectra of a) show the occurrence of precipitated SiO_2 in different concentrations. The lower peak heights in b) at 1224 cm^{-1} correspond to less oxygen

ingot. Typically the oxygen concentration decreases from bottom to the top of the ingots and is particularly high at the bottom. A topographic image of the vertical oxygen distribution is shown in Fig. 1. On the contrary, the concentration of carbon and many other impurities increases from bottom to the top. Depending on the oxygen and carbon concentrations and the cooling rates, particularly in the temperature range between 800 and 1200 °C when the diffusivity is still sufficiently high, both elements may partly precipitate during cooling. Oxygen precipitation is most likely in the bottom part where the concentration is higher. An example is given in Fig. 2 that shows the typical 1224 cm^{-1} band for SiO_2 precipitates. The corresponding concentration of interstitial oxygen in this case shows that more precipitates are formed in as-grown

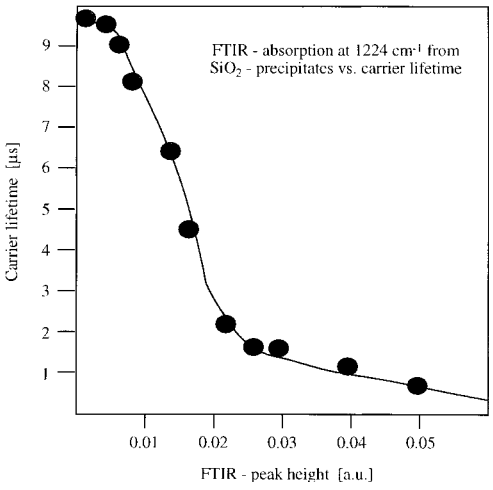

Fig. 3. The carrier lifetime of mc-silicon as a function of the FTIR peak height of the 1224 cm^{-1} band. Although the peak heights cannot be calibrated the result indicate a strong decrease of the lifetime with the amount of precipitated SiO_2

samples when the interstitial oxygen concentration is higher. However, other factors are also important such as the local cooling conditions of the ingot or the concentration of carbon.

An important aspect for the application is that specimens with precipitated oxygen have lower carrier lifetimes compared to specimens with interstitial oxygen only. In Fig. 3 the carrier lifetime, as measured by the μ-PCD method, is depicted as a function of the peak height of the 1224 cm^{-1} band. The results indicate a correlation between the carrier lifetime and the amount of precipitated oxygen. At present it is not possible to calibrate the peak height with a quantity that characterizes the precipitate such as the density, size or shape of SiO_2 precipitates. However, considering that mainly plate-like precipitates are measured here and that oxygen precipitates can occur in various sizes, morphologies or structures, a comprehensive study is certainly necessary to determine the type of precipitate that causes the lifetime reduction. Some preliminary results for this particular material shall be presented in Section 3.3.

3.2 Annealing experiments

The generalization of the results on as grown mc-silicon is hampered by the fact that in most cases the thermal conditions under which commercial ingots have been grown are not available. In order to study the oxygen precipitation under defined conditions annealing experiments have to be carried out. An important problem in this case is however that only as-grown specimens can be used for the annealing experiments. This material has already been thermally treated during the crystallization and cooling process. The annealing results show that the oxygen precipitation depends significantly on the previous thermal treatment of the as-grown specimens which in most cases is unknown as mentioned above. A second factor is the amount of carbon that appears to enhance the formation of SiO_2 precipitates. It is thus not surprising that mc-silicon from various suppliers yields different results after annealing. To obtain reliable results it is therefore necessary to eliminate the thermal history of the samples before carrying out the annealing experi-

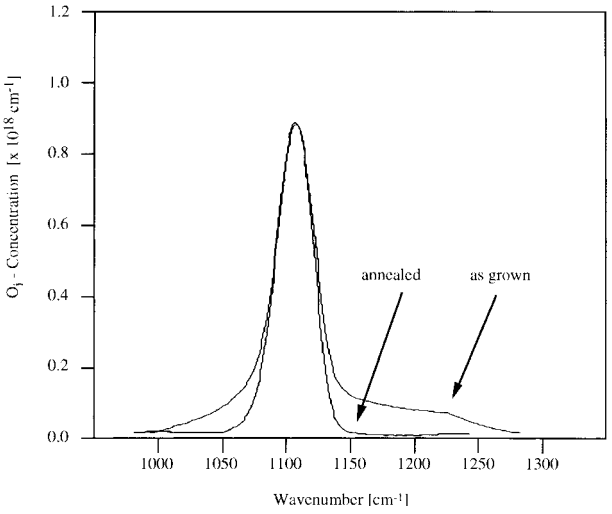

Fig. 4. FTIR spectra of interstitial and precipitated oxygen before and after annealing at 1260 °C for 1 h. The carbon concentration of the investigated specimen is below the FTIR detection limit of 5×10^{15} cm^{-3}

Table 1
Change of interstitial oxygen and carbon concentration in as-grown mc-silicon after annealing at 1260 °C for 1 h. The carbon concentration of the investigated specimen 1 is below the FTIR detection limit of 5×10^{15} cm^{-3}

specimen	oxygen (cm^{-3}) before annealing	oxygen (cm^{-3}) after annealing	carbon (cm^{-3}) before annealing	carbon (cm^{-3}) after annealing
1	8.3×10^{17}	8.2×10^{17}	$<5 \times 10^{15}$	$<5 \times 10^{15}$
2	6.3×10^{17}	7.5×10^{17}	2.3×10^{17}	2.6×10^{17}

ments. The investigations have shown that an annealing step at 1260 °C for 1 h is sufficient to dissolve the precipitates that can be detected by FTIR. This is shown in Fig. 4 for a specimen with a low carbon concentration (below the detection limit of 5×10^{15} cm^{-3}). The precipitate line disappears but very little oxygen is released which indicates that the amount of precipitated oxygen in the as-grown specimen was low in this case. For comparison, the results for a carbon rich material are shown in Table 1.

More oxygen is released into the bulk after annealing in this case which shows that in carbon rich mc-silicon more oxygen has precipitated. Since the dissolved carbon concentration also increases one can assume that in the as-grown material oxygen and carbon co-precipitated. This is in agreement with results for Cz-silicon where carbon also enhances oxygen precipitation [30].

Specimens with low carbon concentrations ($<5 \times 10^{15}$ cm^{-3}) and pre-annealed at 1260 °C for 1 h were used then for the following annealing investigations. This appears to be sufficient to eliminate any previously formed nucleation centers that could enhance the precipitation of oxygen. The specimens were annealed then at different temperatures between 1 and 24 h. Some results are summarized in Fig. 5. The main result is

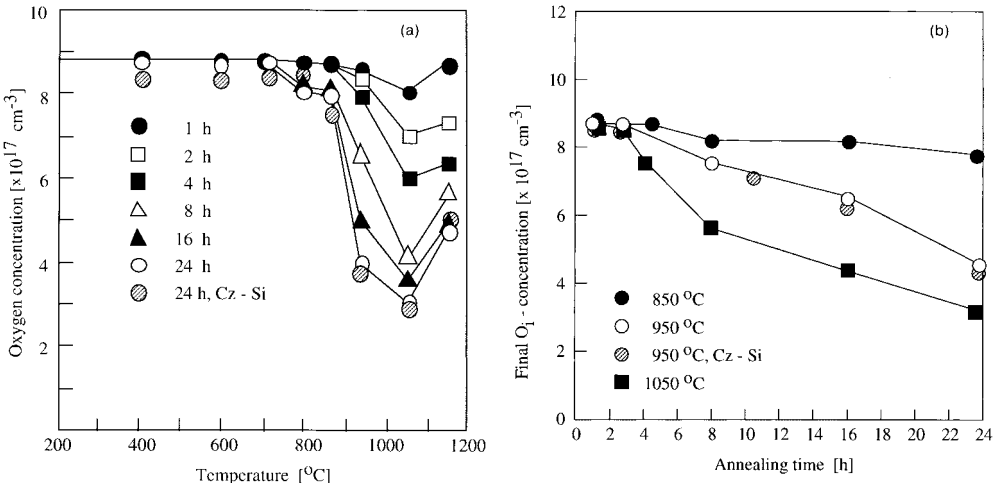

Fig. 5. Concentration of interstitial oxygen in multicrystalline as a function of a) the annealing temperature and b) the annealing time. All specimens have been pre-annealed at 1260 °C for 1 h. For comparison some results for Cz-silicon are included

that for interstitial oxygen concentrations above about 3×10^{17} cm^{-3} the concentration decreases between 750 and 1050 °C. The corresponding FTIR spectra confirm the formation of the SiO_2 phase. However, above 1050 °C the SiO_2 precipitate line at 1224 cm^{-1} disappears again. This indicates that less plate-like and more spherical precipitates are formed above this temperature. This is also confirmed by the TEM investigations (Section 3.3). Below 2×10^{17} cm^{-3} precipitation does not occur anymore. The comparison of the results with pre-annealed Cz-silicon of the same oxygen concentration (and no carbon) shows essentially the same precipitation behavior. Therefore it appears that the presence of dislocations and grain boundaries in mc-silicon has no influence on the precipitation process below that temperature. However, they affect the distribution of precipitates as will be discussed later. Differences occur for mc-silicon with higher carbon concentrations and no pre-annealing. The precipitation rate is enhanced then which suggests that the presence of carbon and the previous annealing treatment during crystallization increases the number of nucleation sites for precipitation. The final amount of precipitated oxygen after a sufficiently long annealing time is less affected, however, the density and size of precipitates are different in these cases.

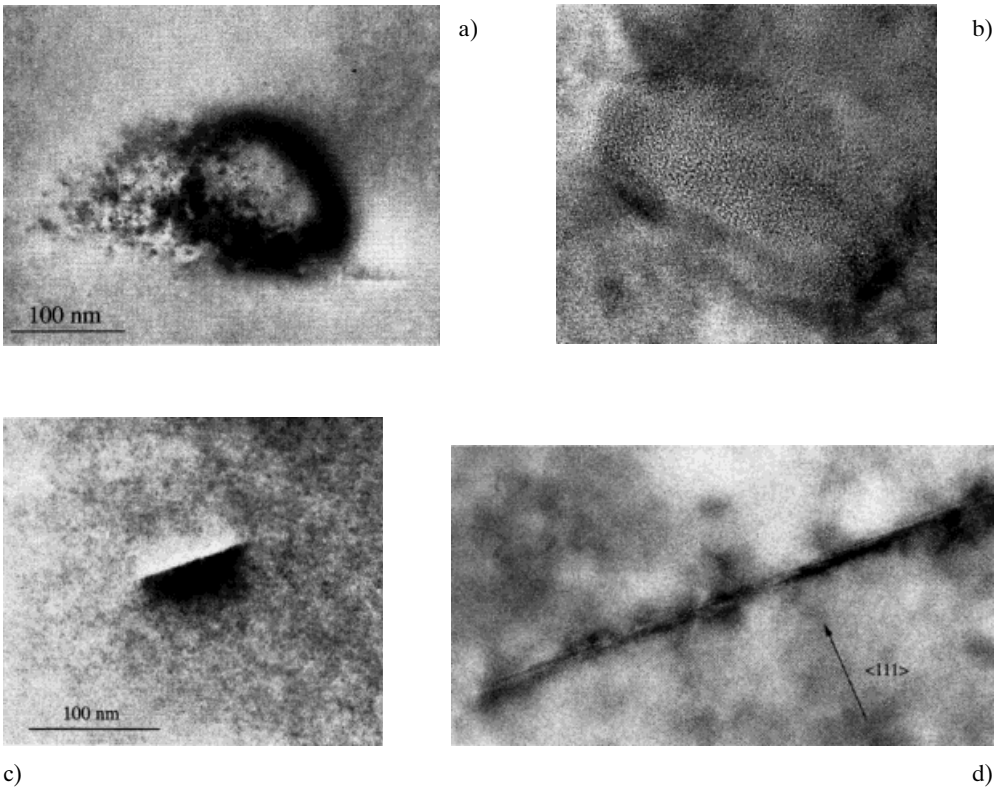

Fig. 6. TEM image of a) a spherical and c) a plate-like SiO_2 precipitate in as-grown mc-silicon. The amorphous structure of the spherical particle is revealed by the HREM image in b). The HREM image of the particle on a (111) plane in d) reveals smaller defects attached to the plate

3.3 TEM investigations

TEM investigations of the same specimens were performed to study the structure of the precipitates in the as-grown and annealed specimens. Basically two types of bulk precipitates are observed: spherical and plate-like defects (Fig. 6). Lattice images confirm the amorphous structure of the spherical defects that are typical for SiO_2 precipitates formed at higher temperatures in Cz-silicon. The sizes vary between 10 and 100 nm depending on the annealing conditions. The plate-like defects on (111) planes have a lateral extension up to 100 nm and a thickness of one or two atomic layers. They could be extrinsic stacking faults but the strong strain field that is always observed suggests that they have to be accompanied by other defects that are difficult to detect. The HREM image of Fig. 6d shows faint strain contrasts that may be due to small oxygen precipitates but the nature of the plate-like defects in general is not clear yet. These plate-like defects are also different from the amorphous silica platelets on (100) planes that are observed in Cz-silicon after moderate annealing in the temperature range 650 to 950 °C [21]. Both spherical and plate-like defects can occur already in the as-grown multicrystalline material with densities up to 10^{11} cm^{-3} depending on the initial oxygen concentration and the thermal conditions during crystal growth. The density increases after annealing in the temperature range between 700 and 1150 °C and can reach maximum values of 10^{12} to 10^{13} cm^{-3} at around 950 °C. Above 1050 °C more spherical precipitates are observed and the 1224 cm^{-1} absorbance line in the FTIR spectra disappears. This could be explained if the plate-like defects contain in fact amorphous SiO_2 that cause the absorption. The transition from plate-like to spherical SiO_2 precipitates at higher temperatures is also observed in Cz-silicon.

Contrary to the oxygen behavior in dislocation free Cz-silicon there is a tendency for oxygen to precipitate at dislocations and grain boundaries in mc-silicon if there is sufficient time to diffuse to the extended defects (Fig. 7). This is the case for higher annealing temperatures and longer annealing times. For instance more decorated dislocations are observed in the bottom region of as-grown ingots that were cooled down slowly. Oxygen decorated dislocations may attract more metal impurities which may explain why they have a higher recombination rate.

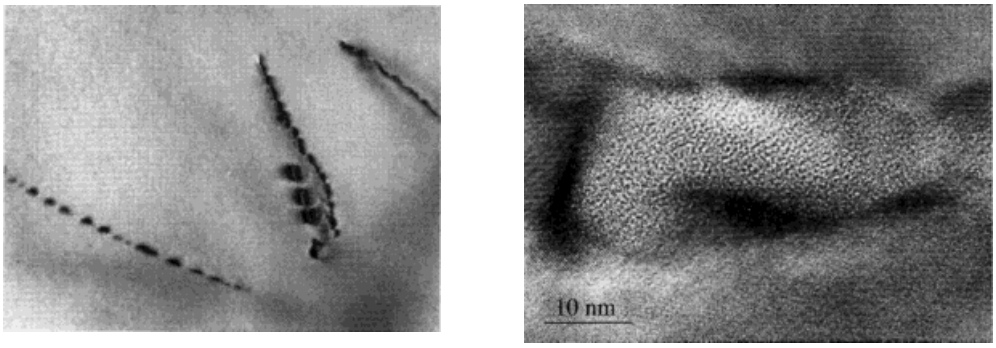

a) b)

Fig. 7. a) Amorphous SiO_2 precipitates at dislocations in annealed mc-silicon. b) HREM image shows the amorphous core of a precipitate at a dislocation

4. Numerical Simulation of the Oxygen Precipitation

4.1 Theoretical description

The experimental results demonstrate that the distribution of oxygen and SiO_2 precipitates depends very much on the processing conditions. Because of the impact on the device performance it is desirable to know the modifications of oxygen which occur for a given sequence of thermal processes. A theoretical model suitable for multi-step annealing processes has to take into account nucleation, growth and the dissolution of precipitates. In recent years it has been shown that a theoretical description based on chemical rate equations can be used to simulate the oxygen precipitation in Cz-silicon numerically [25 to 27, 31 to 33]. The fundamental quantity in the model is a size-distribution function $f(n, t)$ of the precipitate that depends on the number n of oxygen atoms in the precipitate and the time t. The growth of a precipitate containing n atoms is described by a chemical rate equation of the following type (for a complete description of the model see the references)

$$\frac{\partial f(n)}{\partial t} = g(n-1)\, f(n-1) - (d(n) + g(n))\, f(n) + d(n+1)\, f(n+1) \tag{1}$$

with the growth rate $g(n, t)$ and the dissolution rate $d(n, t)$. The condition for particle conservation determines the equation for $n = 1$. For each particle of size n one equation is required. This problem is numerically not tractable for precipitates up to a size of about 100 nm, therefore one has to approximate the equations for larger n by an equation with a continuous variable n. The evaluation of the problem yields the following Focker-Planck type system

$$\frac{\partial f(n)}{\partial t} = \frac{\partial I(n)}{\partial t} \quad \text{with} \quad I(n, t) = -B\, \frac{\partial f(n, t)}{\partial n} + A f(n, t)\,, \tag{2}$$

$$B(n, t) = \frac{1}{2}\, [g(n, t) + d(n, t)]\,, \qquad A(n, t) = g(n, t) - d(n, t) - \frac{\partial B(n, t)}{\partial n}\,. \tag{3}$$

The growth rate $g(n, t)$ and the dissolution rate $d(n, t)$ are given by

$$g(n, t) = k_{\text{react}} C_0^{\text{if}}\,, \quad d(n, t) = k_{\text{react}} C_0^{\text{if, eq}} \quad \text{with} \quad k_{\text{react}} = 4\pi r^2\, \frac{D_0}{\delta}\, \exp\left(\frac{-\Delta G}{kT}\right), \tag{4}$$

$$\Delta G = G(n+1) - G(n) + G_{\text{act}}\,, \qquad G(n) = -nkT \ln\left(\frac{C}{C_0^{\text{eq}}}\right) + 4\pi r^2 \alpha \left(1 + \left(\frac{\zeta}{n}\right)^{1/3}\right), \tag{5}$$

where C_0^{if} and $C_0^{\text{if, eq}}$ are the non-equilibrium and equilibrium concentrations of interstitial oxygen O_i at the precipitate–matrix interface, respectively. $G(n)$ is the Gibbs free energy that describes the chemical driving force for precipitation. In addition, certain boundary conditions are required that are described in detail elsewhere [34]. For the simulation the following parameters are used: the parameter $\zeta = 0.22$ [26], the interfacial energy of the Si/SiO_2 interface $\alpha = 0.48\ \text{J/m}^2$ [35] and $G_{\text{act}} = 0.25$ eV. The temperature dependence of the equilibrium concentration and the diffusion coefficient for oxygen are taken from [36]:

$$C_0^{\text{eq}} = 9 \times 10^{22} \exp\,(-1.52\ \text{eV}/kT)\ (\text{cm}^{-3})\,, \tag{6}$$

$$D_0^{\text{eq}} = 0.13 \exp\,(-2.52\ \text{eV}/kT)\ (\text{cm}^2/\text{s})\,. \tag{7}$$

The theoretical model does not consider the volume expansion (by about a factor of two) and the resulting strains when the SiO_2 phase is formed. It is known that the complexity of oxygen precipitation phenomena in monocrystalline silicon is in fact due to various mechanisms by which the crystal can minimize the total energy of precipitate formation. For instance the strain energy can be reduced by assuming a plate-like shape or by the emission of self-interstitials. The chemical energy can be further reduced by the agglomeration of self-interstitials to stacking faults. In mc-silicon the formation of extrinsic stacking faults has been observed but it is assumed here that in most cases a supersaturation of self-interstitials is less likely because of the many dislocations in mc-silicon that provide enough sinks for the annihilation of self-interstitials. It is further neglected in the calculations that various shapes of precipitates can occur that would require taking into account elastic and anisotropic surface energies.

4.2 Numerical results

In the numerical simulation one has to determine first how many rate equations have to be taken into account before the continuous description by the Focker-Planck equation is sufficient. Since in multi-step annealing processes the small clusters serve as nucleation sites for the further development of larger precipitates one has to determine the number of small clusters quite accurately. For practical reasons one is however limited in the number of differential equations that can be handled numerically. In our case 20 rate equations together with the Focker-Planck equation were solved simultaneously. A larger number of rate equations did not change the final results significantly any more.

The development of the precipitation process shall be discussed for two situations. In the first case a uniform distribution of interstitial oxygen at the beginning is assumed followed by one or two isothermal annealing steps. Experimentally this could only be achieved by a rapid change of the temperature between the annealing steps and particularly after solidification of the crystal. In practice however experiments are usually carried out with as-grown or pre-annealed specimens that have been cooled down slowly to room temperature. The size distribution at the beginning of the annealing treatment is very different in this case as will be shown later. It is therefore assumed in the second case that the specimens have been cooled down slowly from the melting temperature according to an exponential temperature profile before the annealing steps.

4.2.1 Annealing of rapidly cooled specimens

In the first case the oxygen precipitation is simulated for a single annealing step. The calculated size distribution at different annealing temperatures for 1 h annealing is shown in Fig. 8a. An important feature is that the precipitated oxygen occurs in clusters of all sizes. About 10^8 atoms correspond to a precipitate size of about 20 nm assuming a spherical shape. With increasing temperature a peak develops in the size distribution for a cluster size of about 10^6 atoms. In Fig. 8b it is depicted that these large clusters grow on average with increasing annealing time while smaller clusters below about 10^4 atoms shrink. This can be interpreted as the formation of a precipitate in the usual sense because the distribution of the large clusters separates from the small cluster dis-

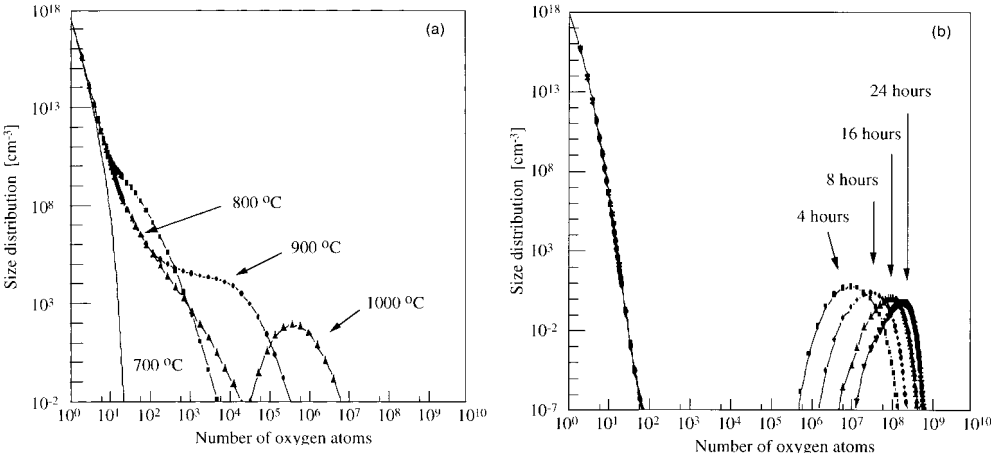

Fig. 8. a) The size distribution $f(n)$ as a function of the particle size n for different annealing temperatures and 1 h annealing time. b) Dependence on the annealing time for the annealing temperature 1050 °C. The initial concentration of interstitial oxygen for the simulation is 1×10^{18} cm^{-3}

tribution. For constant annealing time and temperature the number of precipitates per unit volume (determined from the peak density of large clusters) decreases with the initial oxygen concentration while the size remains more or less the same (Table 2). This explains that below an oxygen concentration of about 5×10^{17} cm^{-3} almost no precipitates can be observed anymore. The results further show that even after a short annealing time a certain number of larger clusters is formed. If a second annealing step follows a re-distribution of the cluster sizes must occur and the question arises how the initial distribution affects the final size distribution. This is shown in Fig. 9 for a two-step annealing process. In this example the second annealing step is kept constant at 1050 °C for 24 h and the first annealing step is varied between 700 and 1000 °C. Compared to the result in Fig. 8b one can see that much higher densities occur for the larger clusters particularly for 1000 °C while the maximum (the average precipitate sizes) shifts to lower values. One can interpret the results in the following way. For a given annealing temperature there exists a critical cluster size above which clusters grow and smaller ones shrink. If the previous annealing treatment has produced more

Table 2

Calculated peak density of SiO_2 clusters as a function of the initial oxygen concentration after annealing at 1050 °C for 24 h. The initial distribution at $t = 0$ is either a step function (rapid cooling) or calculated for a slow cooling process. The average precipitate size in the first cases is about 50 nm and varies in the second case between 20 and 50 nm

oxygen concentration (cm^{-3})	rapid cooling peak density (cm^{-3})	slow cooling peak density (cm^{-3})
12×10^{17}	10^{10}	10^{11}
10×10^{17}	10^{8}	10^{10}
8×10^{17}	10^{5}	10^{9}
6×10^{17}	<10	10^{5}

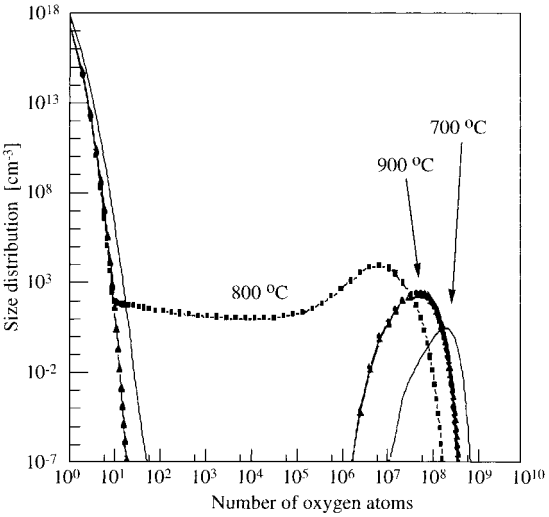

Fig. 9. The size distribution function $f(n)$ for a two step annealing process. The temperature of the first step is varied and the second annealing step is at 1050 °C for 24 h. The initial concentration of interstitial oxygen is 1×10^{18} cm^{-3}

clusters above the critical value the final distribution will have a higher densities of larger clusters. The size distribution above the critical value determines the development of the larger clusters in the following annealing step. This also explains why the annealing conditions during crystal growth are important. They determine the cluster size distribution of as-grown crystals that are usually used for solar cell processing. Other factors that can enhance the formation of clusters such as the presence of carbon are equally important then.

4.2.2 Annealing of slowly cooled specimens

During crystal growth the mc-silicon ingots are solidified and cooled down rather slowly. To simulate the process approximately a cooling profile is assumed where the temperature is reduced exponentially from 1400 °C down to 400 °C. One obtains the size distributions shown in Fig. 10. The slower cooling procedures produce a higher density of larger clusters but no separation of the large cluster distribution. This occurs however after a second annealing step. Compared to the results for an initial distribution of a rapid cooling process in Fig. 8a the peak densities are orders of magnitudes higher here. A similar result can be seen in Table 2 where the dependence on the initial oxygen concentration is compared.

The results also show that for a comparison with experimental data it is necessary to simulate the complete sequence of annealing steps including cooling and heating cycles. In many cases this information is not available. However, one can erase the previous thermal history by a high temperature annealing step. Annealing close to the solubility temperature for the given oxygen concentration will dissolve the large clusters which serve as precursors for the following steps. The experimental results as described in Section 3.2 can therefore be simulated numerically because the following thermal treatments are known. Some of the numerical results are depicted in Fig. 11 for the time dependence of the interstitial oxygen concentration. There is a good agreement with the experimental data.

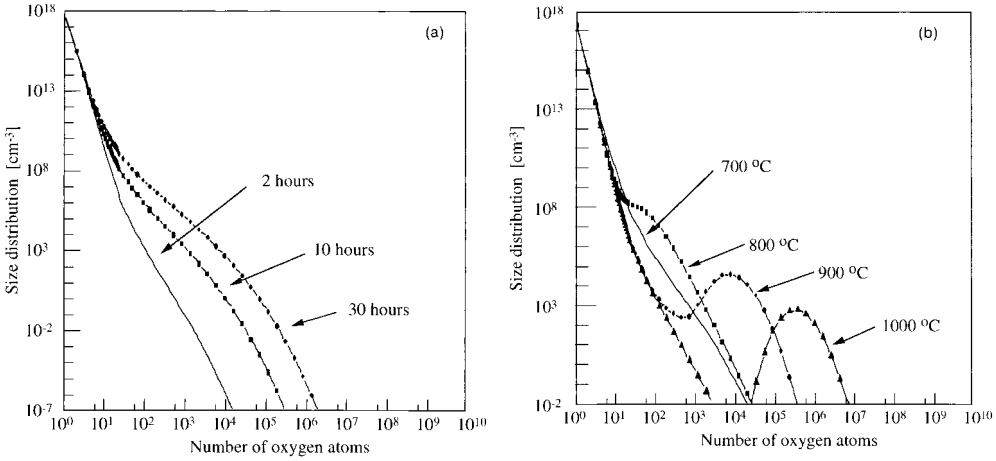

Fig. 10. The size distribution function $f(n)$ for a cooling process from 1400 to 400 °C. A exponential time dependence is assumed in a). In b) an annealing step follows for the 10 h cooling profile. The initial concentration of interstitial oxygen is 1×10^{18} cm^{-3}

5. Summary and Conclusions

The precipitation of oxygen in multicrystalline silicon is enhanced because of a higher density of nucleation centers compared to Cz-silicon. The formation of small oxygen clusters during crystal growth and the presence of carbon have been shown to provide additional nucleation sites. The structure of precipitates and their distribution differs from Cz-silicon. In particular precipitation at dislocations can occur and enhance their recombination activity. Topographic carrier lifetime measurements show that certain SiO_2 precipitates enhance the bulk recombination and are detrimental. A model for the

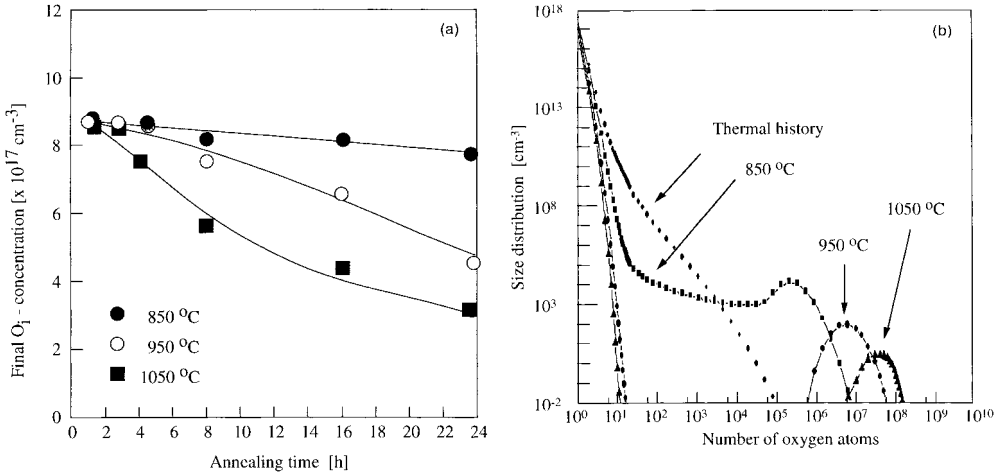

Fig. 11. Calculated concentration of interstitial oxygen as a function of the annealing time. a) The initial concentration of interstitial oxygen is 8.3×10^{17} cm^{-3}. The results are compared with the experimental data given in Fig. 5. b) The corresponding size distributions

precipitation of oxygen in multicrystalline silicon that is based on chemical rate and Focker-Planck equations has been presented. The numerical results have been compared with experimental data of single and two-step annealing processes. A good agreement could be obtained and it could be demonstrated that the model is flexible enough to simulate complex and more realistic annealing procedures.

Acknowledgements Part of the work has been supported by the BMBF under the contract numbers 0329745A and 0329743D. We would like to thank Dr. Müller for supplying the mc-silicon wafers and the results of the μ-PCD measurement.

References

[1] J. M. GEE, R. R. KING, and K. W. MITCHELL, Proc. 25th IEEE Photovoltaic Specialists Conference, Washington (D.C.) IEEE, USA, 1996 (p. 409).
[2] S. PIZZINI, A. SANDRINELLI, M. BEGHI, D. NARDUCCI, F. ALLEGRETTI, S. TORCHIO, G. FABBRI, P. OTTAVIANI, F. DEMARTIN, and A. FISI, J. Electrochem. Soc. **135**, 155 (1988).
[3] B. L. SOPORI, L. JASTRZEBSKI, T. TAN, and S. NARAYANAN, Proc. 12th European Photovoltaic Solar Energy Conf., Amsterdam 1994 H. S. Stephens & Associates, U.K. (p. 1003).
[4] S. A. MCHUGO, H. HIESELMAIR, and E. R. WEBER, Appl. Phys. A **64**, 127 (1997).
[5] C. CABANEL and J. LAVAL, J. Appl. Phys. **67**, 1425 (1990).
[6] M. KITTLER, W. SEIFERT, and V. HIGGS, phys. stat. sol. (a) **137**, 327 (1993).
[7] T. H. WANG, T. F. CISZEK, and T. SCHUYLER, Solar Cells **24**, 135 (1988).
[8] S. A. MCHUGO and W. D. SAWYER, Appl. Phys. Lett. **62**, 2519 (1993).
[9] S. A. MCHUGO, Appl. Phys. Lett. **71**, 1984 (1997).
[10] M. LOGHMARTI, R. STUCK, J. C. MULLER, D. SAYAH, and P. SIFFERT, Appl. Phys. Lett. **62**, 679 (1993).
[11] O. PORRE, M. STEMMER, and M. PASQUINELLI, Mater. Sci. Engng. B **24**, 188 (1994).
[12] B. L. SOPORI, Proc. 20th IEEE Photovoltaic Specialists Conf., Las Vegas 1988 IEEE, USA (p. 591).
[13] J. M. SERRA, R. GAMBOA, A. M. VALERA, A. EYER, and W. WARTA, Proc. 11th European Photovoltaic Solar Energy Conf., Montreux 1992 Harwood Acad. Publ., Switzerland (p. 975).
[14] C. J. VARKER, J. D. WHITFIELD, and P. L. FEJES, Mater. Res. Soc. Symp. Proc. **14**, 187 (1983).
[15] S. W. GLUNZ, S. REIN, W. WARTHA, J. KNOBLOCH, and W. WETTLING, Proc. 2nd World Conf. Photovoltaic Solar Energy Conversion, Vienna 1998.
[16] S. MARTINUZZI and I. PERICHAUD, Mater. Sci. Forum **147**, 1629 (1994).
[17] S. MARTINUZZI, F. FERRAZZA, F. FLORET, I. PERICHAUD, and M. BACON, Proc. 13th European Photovoltaic Solar Energy Conf., Barcelona 1995 H. S. Stephens & Associates, U.K. (p. 975).
[18] K. TEMPELHOFF, F. SPIEGELBERG, R. GLEICHMANN, and D. WRUCK, phys. stat. sol. (a) **56**, 213 (1979).
[19] K. NAUKA, H. C. GATOS, and J. LAGOWSKI, Appl. Phys. Lett. **43**, 241 (1983).
[20] B. R. BATHEY, R. O. BELL, J. P. KALEJS, M. PRINCE, M. D. ROSENBLUM, R. W. STORMONT, and F. V. WALD, see [13] (p. 462).
[21] W. BERGHOLZ, Semiconductors and Semimetals **42**, 513 (1994).
[22] A. BORGHESI, B. PIVAC, A. SASSELLA, and A. STELLA, J. Appl. Phys. **77**, 4169 (1995).
[23] J. MICHEL and L. C. KIMMERLING, Semiconductors and Semimetals **42**, 251 (1994).
[24] H. J. MÖLLER, M. GHOSH, S. RIEDEL, M. RINIO, and D. YANG, see [17] (p. 1390).
[25] M. SCHREMS, T. BRABEC, M. BUDIL, H. PÖTZL, E. GUERRERO, and P. PONGRATZ, Mater. Sci. Engng. B **4**, 393 (1989).
[26] M. SCHREMS, Mater. Sci. Forum **117–118**, 231 (1993).
[27] M. SCHREMS, Semiconductors and Semimetals **42**, 391 (1994).
[28] F. SHIMURA, H. TSUYA, and T. KAWAMURA, Appl. Phys. Lett. **37**, 483 (1980).
[29] S. M. HU, J. Appl. Phys. **51**, 5945 (1980).
[30] For example, see Oxygen, Carbon, Hydrogen and Nitrogen in Crystalline Silicon, Mater. Res. Soc. Symp. Proc. **59** (1986); Semiconductors and Semimetals, Vol. 42, Academic Press, 1994; Defects in Silicon II, The Electrochemical Soc., 1991 and references therein.

[31] L. D. Landau and E. M. Lifshitz, Lehrbuch der theoretischen Physik, Vol. 10, Akademie-Verlag, Berlin 1983 (p. 447).
[32] E. M. Lifshitz and V. Slozov, J. Phys. Chem. Solids **19**, 35 (1959).
[33] R. A. Hatzell, H. F. Schaake, and R. G. Massey, Mater. Res. Soc. Symp. Proc. **36**, 217 (1985).
[34] L. Long and H. J. Möller, to be submitted.
[35] N. Inoue, K. Wada, and J. Osaka, Semiconductor Silicon, The Electrochemical Soc., 1981 (p. 282).
[36] J. C. Mikkelsen, Jr., Mater. Res. Soc. Symp. Proc. **59**, 19 (1986).